Reviews

Structural Similarities among Oxygen-Deficient Perovskites

Mark T. Anderson,† John T. Vaughey,‡ and Kenneth R. Poeppelmeier*

Department of Chemistry and the Science and Technology Center for Superconductivity, Northwestern University, Evanston, Illinois 60208

Received August 24, 1992. Revised Manuscript Received December 14, 1992

A general review and description is given of vacancy patterns in oxygen-deficient perovskites $A_mB_mO_{3m-x}$. Thirteen compounds that contain unique oxygen vacancy patterns and that adopt structures related to cubic closest packing are examined in detail: $m = 2$, $x = 1$, $Ca_2Mn_2O_5$, $LaSrCuGaO_5$, $La_2Ni_2O_5$, $LaSrCuAlO_5$, $YBaCuFeO_5$, $Ca_2Co_2O_5$; $m = 3$, $x = 1$, 2, or 3, $LaBa_2Cu_2TaO_8$, $LaSr_2Fe_3O_8$, $YBa_2Cu_3O_7$, $LnSr_2Cu_2GaO_7$, $YBa_2Cu_3O_6$; $m = 4$, $x = 1$, $Ba_2La_2Cu_2Sn_2O_{11}$ and $Ca_4Ti_2Fe_2O_{11}$. The structural similarity among the compounds is stressed by the presentation and examination of AO_{3-x} slices. The influence of the A and B cations on the manner in which successive AO_{3-x} layers are stacked is presented and discussed.

1. Introduction

The purpose of this review is to systematize and explore the similarities among oxygen-deficient perovskite structures. There are a large number of oxygen-deficient perovskites[1] $A_mB_mO_{3m-x}$ (also $A_nB_nO_{3n-1}$),[2] which encompass a surprising number of vacancy patterns. Many new compounds have been reported since 1986[3] owing to the discovery of high-temperature superconductivity in oxygen-deficient perovskite-related compounds.[4-15] Seven new families of oxygen-deficient perovskites reported since 1986 are included in this review. These are $LaSrCuGaO_5$,[16,17] $LaSrCuAlO_5$,[18,19] $YBaCuFeO_5$,[20-24] $YBa_2Cu_3O_{7-x}$,[4,5,25-27] $LaBa_2Cu_2TaO_8$,[28-30] $LnSr_2Cu_2GaO_7$,[31,32] and $Ba_2La_2Cu_2Sn_2O_{11}$.[33] These are compared with other

† Department of Chemistry, University of California–Santa Barbara, Santa Barbara, CA 93106.

‡ Present address: Department of Chemistry, University of Houston, Houston, TX 77004.

* To whom correspondence should be addressed at the Department of Chemistry.

(1) Rao, C. N. R.; Gopalakrishnan, J. In *New Directions in Solid State Chemistry*; Cambridge University Press: New York, 1989; pp 209–263.

(2) In the notation with m and x, x is required to be an integer. This is convenient way to describe perovskites that have ordered vacancies because m usually corresponds to an integral multiple of the number of perovskite blocks in the unit cell. In the notation with n, the degree of oxygen deficiency is emphasized. The percentage of vacant oxygen sites is simply $100(1/3n)$.

(3) Bednorz, J. G.; Müller, K. A. *Z. Phys. B: Condens. Matter* **1986**, *64*, 189.

(4) Wu, M. K.; Ashburn, J. R.; Torng, C. J.; Hor, P. H.; Meng, R. L.; Gao, L.; Huang, Z. J.; Wang, Y. Q.; Chu, C. W. *Phys. Rev. Lett.* **1987**, *58*, 908.

(5) Beno, M. A.; Soderholm, D. W.; Capone, D. W.; Jorgensen, J. D.; Schuller, K. I.; Serge, C. U.; Zhang, K.; Grace, J. D. *Appl. Phys. Lett.* **1987**, *51*, 57.

(6) Sheng, Z. Z.; Hermann, A. M. *Nature* **1988**, *332*, 55.

(7) Subramanian, M. A.; Torardi, C. C.; Calabrese, J. C.; Gopalkrishnan, J.; Morrissey, J. J.; Askew, T. R.; Flippen, R. B.; Chowdhry, U.; Sleight, A. W. *Nature* **1988**, *332*, 420.

(8) Chu, C. W.; Bechtold, J.; Gao, L.; Hor, P. H.; Huang, Z. J.; Meng, R. L.; Sun, Y. Y.; Wang, Y. Q.; Xue, Y. Y. *Phys. Rev. Lett.* **1988**, *60*, 941.

(9) Hazen, R. M.; Prewitt, C. T.; Angel, R. J.; Ross, N. L.; Finger, L. W.; Hadidacos, C. G.; Veblen, D. R.; Heaney, P. J.; Hor, P. H.; Meng, R. L.; Sun, Y. Y.; Wang, Y. Q.; Xue, Y. Y.; Huang, Z. J.; Gao, L.; Bechtold, J.; Chu, C. W. *Phys. Rev. Lett.* **1988**, *60*, 1174.

(10) Cava, R. J.; Batlogg, B.; Krajewski, J. J.; Rupp, L. W.; Schneemeyer, L. F.; Siegrist, T.; van Dover, R. B.; Marsh, P.; Peck, W. F. Jr.; Gallagher, P. K.; Glarum, S. H.; Marshall, J. H.; Farrow, R. C.; Waszczak, J. V.; Hull, R.; Trevor, P. *Nature* **1988**, *336*, 211.

(11) Sleight, A. W. *Science* **1988**, *242*, 1519.

(12) Rao, C. N. R.; Raveau, B. *Acc. Chem. Res.* **1989**, *22*, 106.

(13) Williams, J. M.; Beno, M. A.; Carlson, K. D.; Geiser, U.; Kao, H. W. I.; Kini, A. M.; Porter, L. C.; Schultz, A. J.; Thorn, R. J.; Wang, H. H.; Whangbo, M.-H.; Evain, M. *Acc. Chem. Res.* **1988**, *21*, 1.

(14) Müller-Buschbaum, H. *Angew. Chem., Int. Ed. Engl.* **1989**, *28*, 1472.

(15) Raveau, B.; Michel, C.; Hervieu, M.; Groult, D. *Springer Series in Materials Science 15, Crystal Chemistry of High-T_c Superconducting Oxides*; Springer-Verlag: New York, 1991.

(16) Vaughey, J. T.; Shumaker, R.; Song, S. N.; Ketterson, J. B.; Poeppelmeier, K. R. *Mol. Cryst. Liq. Cryst.* **1990**, *184*, 335.

(17) Vaughey, J. T.; Wiley, J. B.; Poeppelmeier, K. R. *Z. Anorg. Allg. Chem.* **1991**, *598–599*, 327.

(18) Wiley, J. B.; Markham, L. M.; Vaughey, J. T.; McCarthy, T. J.; Sabat, M.; Hwu, S.-J.; Song, S. N.; Ketterson, J. B.; Poeppelmeier, K. R. In *Chemistry of High-Temperature Superconductors II*; Nelson, D. L., George, T. F., Eds.; Symposium Series No. 377; American Chemical Society: Washington, DC, 1988; p 304.

(19) Wiley, J. B.; Sabat, M.; Hwu, S.-J.; Poeppelmeier, K. R.; Reller, A.; Williams, T. *J. Solid State Chem.* **1990**, *87*, 250.

(20) Er-Rakho, L.; Michel, C.; LaCorre, P.; Raveau, B. *J. Solid State Chem.* **1988**, *73*, 531.

(21) Vaughey, J. T.; Poeppelmeier, K. R. In *Proceedings of the International Electronic Ceramics Conference, Special Publication 804*; National Institute of Standards and Technology; Washington, DC, 1991; p 419.

(22) Meyer, C.; Hartmann-Boutron, F.; Gros, Y.; Strobel, P. *Solid State Commun.* **1990**, *76*, 163.

(23) Pissas, M.; Mitros, C.; Kallias, G.; Psycharis, V.; Niarchos, D.; Simopoulos, A.; Kostikas, A.; Christides, C.; Prassides, K. *Physica C* **1991**, *185–189*, 553.

(24) Pissas, M.; Mitros, C.; Kallias, G.; Psycharis, V.; Simopoulos, A.; Kostikas, A.; Niarchos, D. *Physica C* **1992**, *192*, 35.

(25) Sunshine, S. A.; Murphy, D. W.; Schneemeyer, L. F.; Waszczak, J. V. *Mater. Res. Bull.* **1986**, *22*, 1007.

(26) Bordet, P.; Chaillout, C.; Capponi, J. J.; Chenavas, J.; Marezio, M. *Nature* **1987**, *327*, 687.

(27) Roth, G.; Renker, B.; Hegar, G.; Hervieu, M.; Domengèges, B.; Raveau, B. *Z. Phys. B: Condens. Matter* **1987**, *69*, 53.

(28) Murayama, N.; Sudo, E.; Kani, K.; Tsuzuki, A.; Kawakami, S.; Awano, M.; Torii, Y. *Jpn. J. Appl. Phys.* **1988**, *27*, L1623.

(29) Greaves, C.; Slater, P. R. *Physica C* **1989**, *161*, 245.

(30) Rey, M.-J.; Dehaudt, P.; Joubert, J.; Hewat, A. H. *Physica C* **1990**, *167*, 162.

(31) Vaughey, J. T.; Thiel, J. P.; Groenke, D. A.; Stern, C. L.; Poeppelmeier, K. R.; Dabrowski, B.; Hinks, D. G.; Mitchell, A. W. *Chem. Mater.* **1991**, *3*, 935.

(32) Roth, G.; Adelmann, P.; Hegar, G.; Knitter, R.; Wolf, Th. *J. Phys.* **1991**, *1*, 721.

(33) Anderson, M. T.; Zhang, J. P.; Poeppelmeier, K. P.; Marks, L. D. *Chem. Mater.*, in press.

0897-4756/93/2805-0151$04.00/0

transition-metal oxygen-deficient compounds reviewed by Rao[1] and Gopalakrishnan in 1984, $Ca_2Mn_2O_5$,[34,35] $La_2Ni_2O_5$,[36,37] and $Ca_2Co_2O_5$,[38] and with the recently discovered transition-metal compounds $LaSr_2Fe_3O_8$,[39-42] and $Ca_4Fe_2Ti_2O_{11}$.[43]

The structural similarity among oxygen-deficient perovskites, especially those with the same general formula, is not obvious when the compounds are viewed as three-dimensional arrangements of ions or as assemblies of polyhedra. Nor is it obvious why such a diverse array of vacancy patterns exists. To systematize oxygen-deficient perovskite structures and expose similarities among them, we reduce all oxygen-deficient perovskites to a fundamental building block that can be compared, contrasted, and arranged in different manners to generate a variety of oxygen vacancy patterns and three-dimensional structures. The fundamental block is the AO_{3-x} layer. We show that what appear to be unrelated structures can be constructed from topologically related (section 3.3) AO_{3-x} layers by stacking the layers in different manners. To generate a particular three-dimensional structure, identical AO_{3-x} layers are stacked and B cations are placed in one-fourth of the octahedral ($x = 0$) interstices between the layers. The process yields an ...AO_{3-x}B AO_{3-x}B AO_{3-x}... sequence perpendicular to the AO_{3-x} layers in which the A and O are approximately cubic closest packed. The coordination, electronic structure, and metal–oxygen bond lengths of the A and B cations are the primary factors that control the manner in which the layers stack and differences in these parameters lead to a diverse array of vacancy patterns.

In this paper we review the vacancy patterns for $A_mB_mO_{3m-x}$ oxygen-deficient perovskites. We examine six unique vacancy arrangements found for $A_2B_2O_5$ ($m = 2$), five found for $A_3B_3O_{9-x}$ ($m = 3$; $x = 1$, 2, or 3), and two found for $A_4B_4O_{11}$ ($m = 4$) compounds. Polyhedral representations are compared and contrasted with their equivalent close-packed AO_{3-x} models to better appreciate and understand the nature of oxygen deficiency in these seemingly diverse and unrelated compounds.

2. Review of Oxygen-Deficient Perovskites

2.1. Perovskite Structure. The perovskite structure can be described as a $BO_{6/2}$ framework of corner-shared octahedra that contains A cations within 12-coordinate sites; see Figure 1. An oxygen-deficient perovskite structure can be described as a $BO_{6/2-x/2}$ framework, wherein some of the A and B cations are less than 12- and 6-coordinate, respectively. This particular description emphasizes the dimensionality, local A and B cation coordination, and overall symmetry of the compounds. Alternatively, the perovskite structure can be described as a cubic-close-packed arrangement of AO_3 layers between which one-fourth of the octahedral interstices are filled by B cations; see Figure 2. We propose a similar description of oxygen-deficient perovskites as close-packed ABO_{3-x} layers. This description emphasizes the ionic bonding and three-dimensional structural similarity of the compounds.

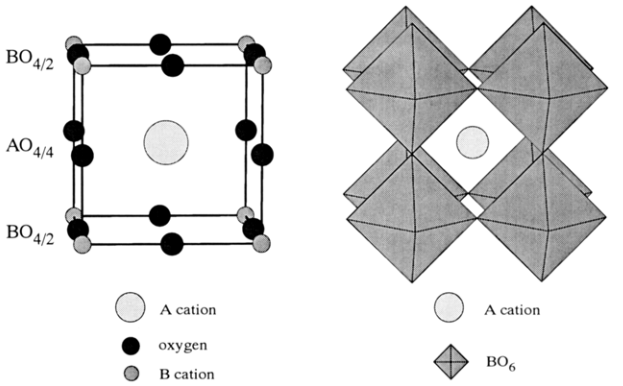

Figure 1. Two depictions of the ideal perovskite structure.

2.2. Two General Formulas. Two general formulas will be used to categorize oxygen-deficient perovskites, $A_mB_mO_{3m-x}$ and $A_nB_nO_{3n-1}$. The former will be used to emphasize structural similarity, and the latter to facilitate comparison of the degree of oxygen deficiency among compounds. Note that the percentage of vacant sites in the latter notation is simply $100(1/3n)$. The $A_mB_mO_{3m-x}$ notation provides a convenient way to describe perovskites that have ordered vacancies. In this notation, x is an integer and therefore m is an integral multiple of the number of perovskites blocks in the unit cell. The notation will be used extensively to group compounds into those derived from double perovskites ($m = 2$, $A_2B_2O_{6-x}$), triple perovskites ($m = 3$, $A_3B_3O_{9-x}$), quadruple perovskites ($m = 4$, $A_4B_4O_{12-x}$), and compounds that have larger repeats ($m > 4$). The equivalent $A_nB_nO_{3n-1}$ notation will be provided by each example to emphasize the degree of reduction. As n decreases, the number of vacancies increases.

2.3. Concentration and Arrangement of Vacancies. In general, ordered oxygen-deficient perovskites $A_nB_nO_{3n-1}$ exist for $n = 1$ to ∞, that is, $ABO_{2.00}$ to $ABO_{3.00}$. Compounds that contain ordered oxygen vacancies are known for $n = 5$, 4, 3, 2, 1.5, 1.33, and 1, that is, overall oxygen contents of 2.80, 2.75, 2.67, 2.50, 2.33, 2.25, and 2.00 for $ABO_{3-\delta}$. Oxygen atoms are generally removed from $[100]_c$ or $[110]_c$ rows or $(001)_c$ planes (see Figure 3), and in the case of very deficient structures the vacancies are removed from a row and a plane. Removal of oxygen atoms from $[100]_c$ rows results in the formation of MO_5 square pyramids or MO_4 square planes, removal from $[110]_c$ rows results in the formation of MO_4 tetrahedra, and removal from $(100)_c$ planes results in MO_5 square pyramids. The compounds in Table I demonstrate the diversity of vacancy patterns and coordination polyhedra found in oxygen-deficient perovskites.

2.4. Polyhedral Descriptions of $A_mB_mO_{3m-x}$ Oxygen-Deficient Perovskite Structures. The descriptions emphasize the relationship to the aristotype, that is, the manner in which the oxygen atoms have been removed from stoichiometric perovskite. Some of the cells have a

(34) Poeppelmeier, K. R.; Leonowicz, M. E.; Longo, J. M. *J. Solid State Chem.* **1982**, *44*, 89.
(35) Poeppelmeier, K. R.; Leonowicz, M. E.; Scanlon, J. C.; Longo, J. M.; Yelon, W. B. *J. Solid State Chem.* **1982**, *45*, 71.
(36) Rao, C. N. R.; Gopalkrishnan, K.; Vidyasagar, K.; Ganguli, A. K.; Ramanan, A.; Ganapathi, L. *J. Mater. Res.* **1986**, *1*, 280.
(37) Vidyasagar, K.; Reller, A.; Gopalakrishnan, J.; Rao, C. N. R. *J. Chem. Soc., Chem. Commun.* **1985**, 7.
(38) Vidyasagar, K.; Gopalakrishnan, J.; Rao, C. N. R. *Inorg. Chem.* **1984**, *23*, 1206.
(39) Battle, P. D.; Gibb, T. C.; Lightfoot, P. *J. Solid State Chem.* **1990**, *84*, 237.
(40) Battle, P. D.; Gibb, T. C.; Nixon, S. *J. Solid State Chem.* **1989**, *79*, 75.
(41) Battle, P. D.; Gibb, T. C.; Nixon, S. *J. Solid State Chem.* **1988**, *77*, 124.
(42) Battle, P. D.; Gibb, T. C.; Nixon, S. *J. Solid State Chem.* **1988**, *79*, 86.
(43) González-Calbet, J. M.; Vallet-Regí, M. *J. Solid State Chem.* **1987**, *68*, 266.

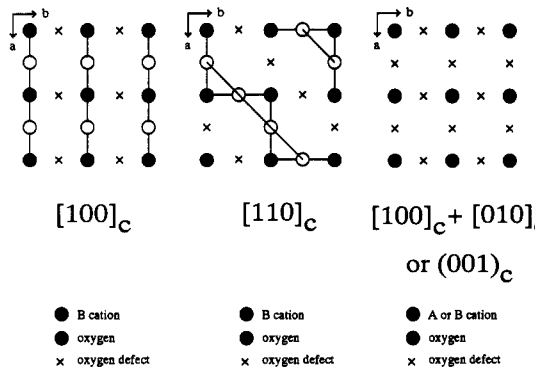

Figure 3. Three common oxygen defect patterns found in oxygen-deficient perovskites.

$\sqrt{2}a_p$ or larger expansion of two axes. The expansion of the cells results from displacements of oxygen atoms, order of oxygen vacancies, or both. Large supercells can result if both mechanisms are operational.[33] The notation a_p refers to the unit cell edge of cubic perovskite, which is typically 3.8–4.1 Å.

2.4.1. m = 2. No less than six vacancy patterns are known for $A_2B_2O_5$ oxygen-deficient perovskites. The most common structure type is brownmillerite, which is named for the mineral with the composition Ca_2FeAlO_5[44,45] and is exhibited by $Ca_2Fe_2O_5$[46,47] along with many others.

$LaSrCuGaO_5$[16,17] (n = 2), which has the brownmillerite structure, is orthorhombic and has a $4a_p \times \sqrt{2}a_p \times \sqrt{2}a_p$ cell size; see Figure 4. It has oxygen atoms removed from alternate [001], i.e., $[110]_c$, rows in every other (100) $BO_{4/2}$ plane. The rows of vacancies are staggered as viewed down [100]. The CuGaCuGaCu coordination polyhedra are OTOT′O parallel to the a axis (where O is octahedral and T is tetrahedral; the prime indicates a different orientation of the second tetrahedron relative to the first).

The $LaSrCuAlO_5$[18,19] (n = 2) structure is similar to the brownmillerite structure; see Figure 5. $LaSrCuAlO_5$ is orthorhombic and the cell size is $2a_p \times 2\sqrt{2}a_p \times \sqrt{2}a_p$. As in $LaSrCuGaO_5$, the oxygen atoms are removed from alternate [001], i.e., $[110]_c$, rows in every other (100) $BO_{4/2}$ plane. In contrast to $LaSrCuGaO_5$, the rows of vacancies are stacked above one another as viewed down [100], which halves the a-axis length with respect to the gallate. The CuAlCuAlCu coordination polyhedra are STSTS parallel to the a axis (where S is square pyramidal). The copper is pseudo-six-coordinate, with a sixth copper–oxygen distance of 2.954 (8) Å.

$Ca_2Mn_2O_5$[34,35] (n = 2) and $La_2Ni_2O_5$[36,37] (n = 2) have oxygen atoms removed from [001] and [100] rows, respectively. $Ca_2Mn_2O_5$ is orthorhombic and the cell size is $\sqrt{2}a_p \times 2\sqrt{2}a_p \times 1a_p$; see Figure 6. The oxygen atoms are removed from every fourth [001] row in each $AO_{4/4}$ plane and $BO_{4/2}$ plane, and all of the d^4 manganese atoms have square-pyramidal coordination. As can be seen in Figure 6, when viewed along ⟨120⟩ the oxygen atoms are removed from the right, left, back, front, right, left, back, front of successive MnO_6 polyhedra. The structure type is also known for $La_2Cu_2O_5$[48] and for $Ba_2Bi_2O_5$.[49] $La_2Ni_2O_5$ is tetragonal and the cell size is $1a_p \times 1a_p \times 4a_p$; see Figure 7. The oxygen atoms are removed from every [100] row in every other (001) $BO_{4/2}$ plane. The nickel coordination polyhedra are OPOPO parallel to the c axis (where P is square planar).

$YBaCuFeO_5$[20–24] (n = 2; also its cobalt analog)[50] is tetragonal and has a $1a_p \times 1a_p \times 2a_p$ cell size. The oxygen atoms are removed from every other (001) $AO_{4/4}$ plane (see Figure 8), which contrasts with the four compounds above where the oxygen atoms are removed from $[100]_c$ or $[110]_c$ rows in $BO_{4/2}$ planes. The copper and iron have square-pyramidal coordination. The degree of order of the copper and iron is in question, but it appears[21,22] that they are ordered and form $CuO_{4/2}$ and $FeO_{4/2}$ planes that alternate parallel to the c axis.

$Ca_2Co_2O_5$[38] (n = 2) is orthorhombic and has a $2\sqrt{2}a_p \times 2\sqrt{2}a_p \times 2a_p$ cell size. All of the cobalt atoms are reported to have square pyramidal coordination; see Figure 9. The vacancy pattern is more complex than for the other $A_2B_2O_5$ compounds. Every other (001) $BO_{4/2}$ plane has the same vacancy pattern[38] as $Ca_2Mn_2O_5$, that is, when viewed along ⟨220⟩, the oxygen atoms are removed from the right, left, back, front, right, left, back, front of successive CoO_6 polyhedra. In the other (001) $BO_{4/2}$ planes, the oxygen atoms are removed from alternate sides (left, right, left, right) of successive CoO_6 polyhedra as viewed along ⟨220⟩.

2.4.2. m = 3. $A_3B_3O_{9-x}$ oxygen-deficient compounds have overall oxygen contents that range from 6.00 to 9.00 (x = 3 to 0). Except for $Ca_2LaFe_3O_8$,[39–42] $A_3B_3O_{9-x}$ compounds have oxygen atoms completely removed from every third $(001)_c$ $AO_{4/4}$ plane. The vacancy patterns in all but $Ca_2LaFe_3O_8$ are similar to $YBaCuFeO_5$, in which all of the oxygen atoms are removed from every other $(001)_c$ $AO_{4/4}$ plane.

The end members in the 123 Y–Ba–Cu–O[4,5] system, $YBa_2Cu_3O_6$ and $YBa_2Cu_3O_7$, have distinct vacancy patterns. $YBa_2Cu_3O_6$[25–27] (n = 1) is tetragonal, has a $1a_p \times 1a_p \times 3a_p$ cell size, and has oxygen atoms removed from every third (001) $AO_{4/4}$ plane and every third (001) $BO_{4/4}$ plane; see Figure 10. The coordination around copper is SLS SLS parallel to the c axis (where S is square pyramidal and L is linear). $YBa_2Cu_3O_7$[4,5] (n = 1.5) is orthorhombic and has a $1a_p \times 1a_p \times 3a_p$ cell. It has oxygen atoms removed from every third (001) $AO_{4/4}$ plane, and has oxygen atoms removed from every [100] row in every third (001) $BO_{4/4}$ plane; see Figure 11. The copper coordination polyhedra are SPS SPS parallel to the c axis (where S is square pyramidal and P is square planar).

$LaBa_2Cu_2TaO_8$[28–30] (n = 3; and its niobium analog)[30] is tetragonal and has a $1a_p \times 1a_p \times 3a_p$ subcell. The structure of the tantalate is similar to $YBa_2Cu_3O_7$ except that tantalum has replaced the chain copper atom and is six-coordinate rather than four-coordinate; see Figure 12. It has oxygen atoms removed from every third (001) $AO_{4/4}$ plane. The CuTaCu CuTaCu coordination polyhedra are SOS SOS parallel to the c axis. The actual cell size is $\sqrt{2}a_p \times \sqrt{2}a_p \times 6a_p$ owing to rotations of the TaO_6 octahedra.[30]

(44) Hansen, W. C.; Brownmiller, L. T.; Bogue, R. H. *J. Am. Chem. Soc.* **1928**, *50*, 396.
(45) Colville, A. A.; Geller, S. *Acta Crystallogr., Sect B* **1971**, *27*, 2311.
(46) Bertaut, E. F.; Blum, P.; Sagnieres, A. *C. R. Acad. Sci. (Paris)* **1957**, *244*, 2944.
(47) Colville, A. A. *Acta Crystallogr., Sect B* **1970**, *26*, 1469.
(48) Bringley, J. F.; Scott, B. A.; LaPlaca, S. J.; Boehme, N. F.; Shaw, T. M.; McElfresh, W. W.; Trail, S. S.; Cox, D. E. *Nature* **1990**, *347*, 263.
(49) Lightfoot, P.; Hriljac, J. A.; Pei, S.; Zhang, Y.; Mitchell, A. W.; Richards, D. R.; Dabrowski, B.; Jorgensen, J. D.; Hinks, D. G. *J. Solid State Chem.* **1991**, *92*, 473.
(50) Barbey, L.; Nguyen, N.; Caignaert, V.; Hervieu, M.; Raveau, B. *Mater. Res. Bull.* **1992**, *27*, 295.

Table I. Oxygen-Deficient Perovskites[a]

$A_mB_mO_{3m-x}$	c.n. B cations	c.n. A cations	cell size	B–O polyhedra, electron config.	AO_{3-x} pattern	ref
			$m = 2$			
$Ca_2Mn_2O_5$	5, 5	10, 10	a = 5.424(2) b = 10.230(4) c = 3.735(2)	SSSS d^4, d^4	AO O□ AO O_2 AO □O AO O_2	34
$LaSrCuGaO_5$	6, 4	8, 8	a = 16.383(1) b = 5.5293(7) c = 5.3275(6)	OTOT′ d^9, d^{10}	AO O□ AO O_2 AO □O AO O_2	17
$La_2Ni_2O_5$	6, 4	10, 10	a = 7.816[b] c = 7.468	OPOP d^8, d^8	AO O□ AO O_2	37
$LaSrCuAlO_5$	5, 4	8, 9	a = 7.9219(6) b = 11.020(1) c = 5.4235(4)	STST′ d^9, d^{10}	AO O□ AO O_2	19
$YBaCuFeO_5$	5, 5	8, 12	a = 3.893(2) c = 7.751(3)	SSSS d^9, d^5	AO O_2 A□ O_2	20
$Ca_2Co_2O_5$	5, 5	8-12	a = 11.12(1) b = 10.74(1) c = 7.48(1)	SSSS d^6, d^6	AO O□ AO $O_{1.5}$□$_{0.5}$ A□ $O_{1.5}$□$_{0.5}$ AO O_2 AO O_2 $AO_{0.5}$□$_{0.5}$ O_2	38
			$m = 3$			
$YBa_2Cu_3O_6$	5, 5, 2	8, 8, 8	a = 3.8715(6) c = 11.738(2)	SLS SLS d^9, d^{10}, d^9	AO □$_2$ AO O_2 □A O_2 AO □$_2$ AO O_2 A□ O_2	26
$YBa_2Cu_3O_7$	5, 5, 4	8, 10, 10	a = 3.8231(1) b = 3.8864(4) c = 11.6807(2)	SPS SPS d^9, d^8, d^9	AO O□ AO O_2 □A O_2 AO □O AO O_2 A□ O_2	5
$LaBa_2Cu_2TaO_8$	5, 5, 6	8, 12, 12	a = 5.6107(2) c = 23.9863(4)	SOS SOS d^9, d^0, d^9	AO O_2 AO O_2 □A O_2 AO O_2 AO O_2 A□ O_2	30
$LnSr_2Cu_2GaO_7$	5, 5, 4	8, 8, 8	a = 22.1425(9) b = 5.5662(2) c = 5.4648(2)	STS ST′S d^9, d^{10}, d^9	AO O□ AO O_2 □A O_2 AO □O AO O_2 A□ O_2	31
$LaSr_2Fe_3O_8$	6, 6, 4	12, 8, 8	a = 5.5095(1) b = 11.8845(5) c = 5.6028(1)	OTO OT′O d^5, d^5, d^5	AO O_2 AO O□ AO O_2	39
			$m = 4$			
$Ba_2La_2Cu_2Sn_2O_{11}$	5, 5, 6, 6	12, 12, 12, 8	a = 3.98[b] c = 16.23	SOOS SOOS d^9, d^{10}, d^{10}, d^9	AO O_2 AO O_2 A□ O_2 AO O_2	33
$Ca_4Ti_2Fe_2O_{11}$	6, 6, 6, 4	10, 12, 12, 10	a = 5.437(1) b = 30.22(1) c = 5.489(1)	OTOO OT′OO d^0, d^5, d^0, d^5	AO O□ AO O_2 AO O_2 AO O_2	43

[a] O, octahedral; S, square pyramidal; P, square planar; T, tetrahedral; L, linear. [b] Errors not given.

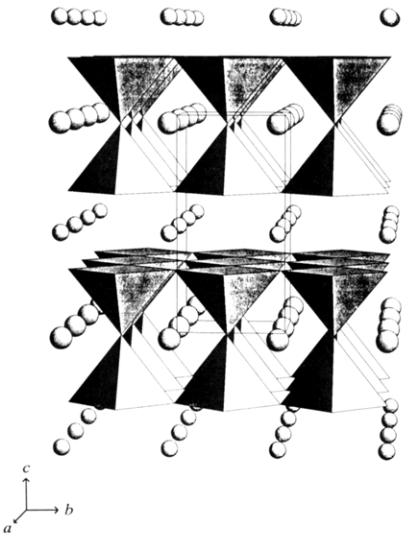

Figure 8. Structure of $YBaCuFeO_5$. The square pyramids are CuO_5 and FeO_5. The larger spheres are barium and the smaller are yttrium.

$LnSr_2Cu_2GaO_7$[31,32] (n = 1.5; also its cobalt analog)[51] is orthorhombic and has a $6a_p \times \sqrt{2}a_p \times \sqrt{2}a_p$ cell size. It has oxygen atoms removed from every third (100) $AO_{4/4}$ plane, and has oxygen atoms removed from alternate [001],

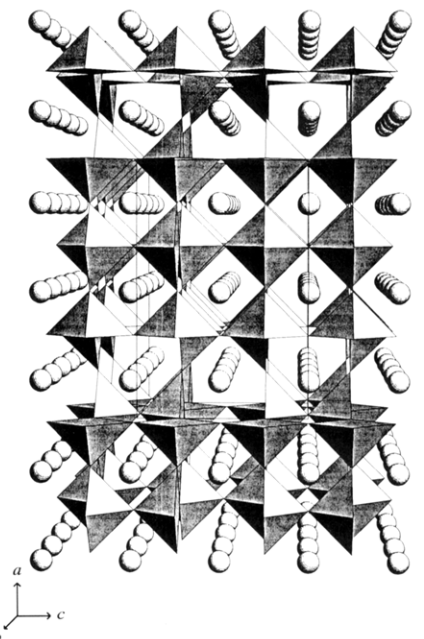

Figure 9. Proposed structure of $Ca_2Co_2O_5$ after Vidyasagar et al.[38] The square pyramids are CoO_5 and the spheres are calcium.

i.e., $[110]_c$, rows in every third (100) $BO_{4/4}$ plane; see Figure 13. The rows of [001] vacancies are staggered from $GaO_{2/2}$ plane to $GaO_{2/2}$ plane, as in $LaSrCuGaO_5$.[17,18] The CuGaCu CuGaCu coordination polyhedra are STS ST′S parallel to the a axis.

(51) Huang, Q.; Cava, R. J.; Santoro, A.; Krajewski, J. J.; Peck, W. F. *Physica C* **1992**, *193*, 196.

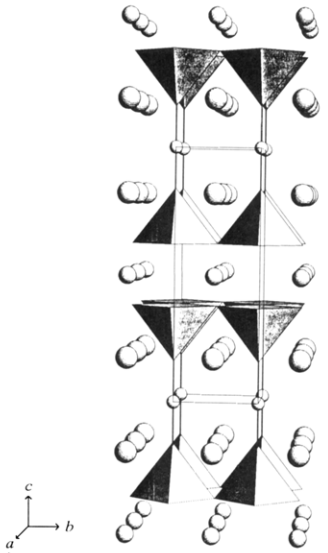

Figure 10. Structure of $YBa_2Cu_3O_6$ after Bordet et al.[26] The square pyramids are CuO_5. The smallest spheres are copper, the intermediate spheres are yttrium, and the largest spheres are barium.

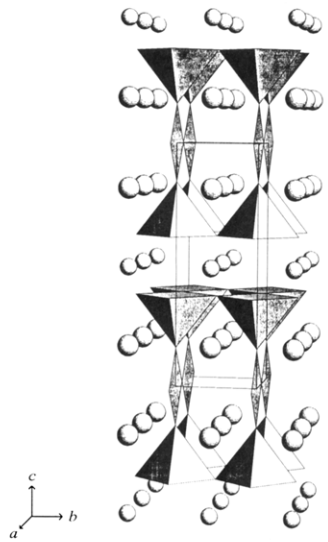

Figure 11. Structure of $YBa_2Cu_3O_7$ after Beno et al.[5] The square planes are CuO_4 and the square pyramids are CuO_5. The smaller spheres are yttrium, and the larger spheres are barium.

$LaSr_2Fe_3O_8$[39-42] (n = 3; also $LaCa_2Fe_3O_8$[52] and $Ca_3Fe_2TiO_8$[53]) is orthorhombic and has a $\sqrt{2}a_p \times 3a_p \times \sqrt{2}a_p$ cell size. It has oxygen atoms removed from alternate [100], i.e., $[110]_c$, rows in every third (010) $BO_{4/4}$ plane similar to $LnSr_2Cu_2GaO_7$; see Figure 14. The iron coordination polyhedra are OTO OTO parallel to the b axis (perpendicular to the $FeO_{4/2}$ chains), which contrasts with $LnSr_2Cu_2GaO_7$ in which the tetrahedra have different orientations, T and T′, perpendicular to the $GaO_{4/2}$ chains.

2.4.3. m = 4. The compounds in this class have the formula $A_4B_4O_{11}$ (n = 4). Compounds include $Sr_4Sr_2Ta_2O_{11}$[54] (also with barium), $Ba_4Ta_2Cd_2O_{11}$, and $Ba_4Ce_2In_2O_{11}$,[55] $Ca_4Fe_2Ti_2O_{11}$,[43] and $Ba_2La_2Cu_2Sn_2O_{11}$.[33] The last two have been characterized by diffraction techniques and electron microscopy. $Ca_4Fe_2Ti_2O_{11}$[43] (n = 4) is orthorhombic and has a $\sqrt{2}a_p \times 8a_p \times \sqrt{2}a_p$ cell size. The structure is not shown. It has been proposed that the oxygen vacancy pattern is similar to that for $LaCa_2Fe_3O_8$,[52] but there is one more octahedron per formula unit (see section 2.4.2). The compound has oxygen atoms removed from alternate [101] rows, i.e., $[110]_c$, in every fourth (010) $BO_{4/2}$ plane, and, assuming the iron and titanium cations are ordered, the TiFeTiFe TiFeTiFe coordination polyhedra are OTOO OTOO parallel to the b axis. $Ba_2La_2Cu_2Sn_2O_{11}$[33] (n = 4) is tetragonal, has a $1a_p \times 1a_p \times 4a_p$ subcell, see Figure 15, and has a modulated structure that has a periodicity of roughly $\sqrt{2}a_p \times \sqrt{2}a_p \times 24a_p$. Oxygen atoms are removed from one-half of the (001) $AO_{4/4}$ planes, and the CuSnSnCu CuSnSnCu coordination polyhedra are SOOS SOOS parallel to the c axis. The compound is similar to $LaBa_2Cu_2TaO_8$[28-30] except that there are two corner-shared octahedral tin layers rather than one corner-shared octahedral tantalum layer.

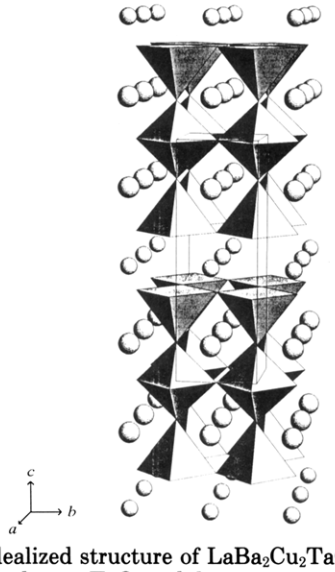

Figure 12. Idealized structure of $LaBa_2Cu_2TaO_8$ after Rey et al.[30] The octahedra are TaO_6 and the square pyramids are CuO_5. The smaller spheres are lanthanum and the larger are barium.

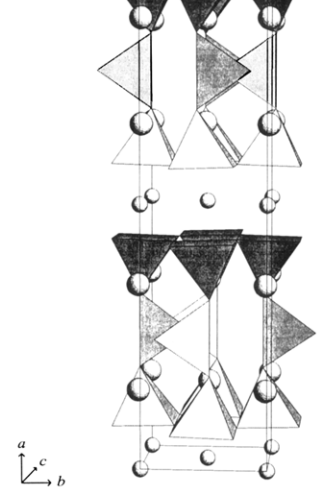

Figure 13. Structure of $LnSr_2Cu_2GaO_7$. The tetrahedra are GaO_4 and the square pyramids are CuO_5. The smaller spheres are yttrium and the larger are strontium.

(52) Grenier, J. C.; Menil, F.; Pouchard, M.; Hagenmuller, P. *Mater. Res. Bull.* **1977**, *12*, 79.
(53) Rodriguez-Carvajal, J.; Vallet-Regi, M.; Gonzalez-Calbet, J. M. *Mater. Res. Bull.* **1989**, *24*, 423.
(54) Brixner, L. *J. Am. Chem. Soc.* **1958**, *80*, 3214.
(55) Jacobson, A. J.; Collins, B. M.; Fender, B. E. F. *Acta Crystallogr., Sect B* **1976**, *32*, 1083.

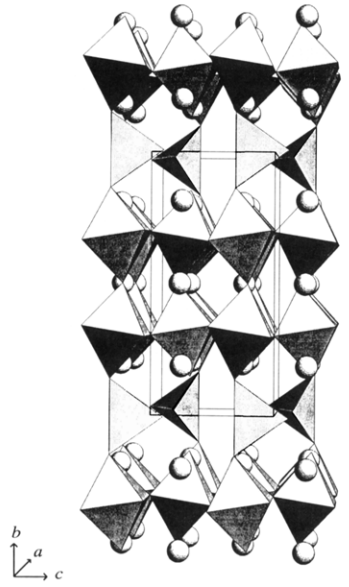

Figure 14. Structure of $LaSr_2Fe_3O_8$ after Battle et al.[39] The tetrahedra are FeO_4 and the octahedra are FeO_6. The spheres are lanthanum and strontium.

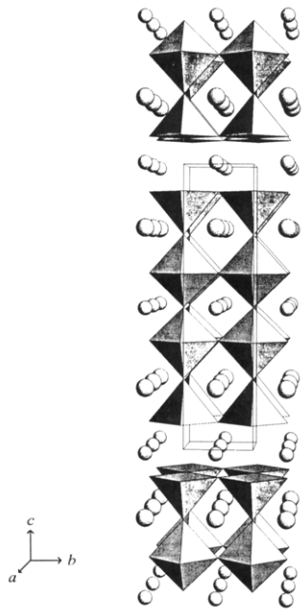

Figure 15. Structure of $Ba_2La_2Cu_2Sn_2O_{11}$. The octahedra are SnO_6 and the square pyramids are CuO_5. The smaller spheres are lanthanum and the larger are barium.

2.4.4. $m > 4$. There are many compounds that have more complicated vacancy patterns, most of which have been examined only by electron microscopy. Short-range order of vacancies and the presence of microdomains are common in $m > 4$ compounds. A variety of complex compounds will be included in sections 2.4.4–2.4.6 for completeness, but their vacancy patterns will not be examined in detail.

The solid solution $CaTi_{1-2y}Fe_{2y}O_{3-y}$[56] contains a series of intergrowth structures, all of which have orthorhombic crystal symmetry when y is greater than 0.25. The compounds have m values close to definite compositions. Compounds with the formulas $Ca_5TiFe_4O_{13}$ ($y = 0.40$, $n = 2.5$), $Ca_7Ti_3Fe_4O_{19}$ ($y = 0.29$, $n = 3.5$), $Ca_7TiFe_6O_{18}$ ($y = 0.43$, $n = 2.33$), $Ca_8Ti_2Fe_6O_{21}$ ($y = 0.37$, $n = 2.67$), and $Ca_{11}TiFe_{10}O_{28}$ ($y = 0.45$, $n = 2.2$) have been identified. All show evidence of ordered vacancies and have intergrown structures that do not have a definite order of the various microdomains. $Ca_4YFe_5O_{13}$[57] ($n = 2.5$) is orthorhombic and exhibits regular intergrowths of $n = 2$ and $n = 3$ units, and, as determined from electron microscopy, has an OOTOT OOTOT sequence of iron coordination polyhedra. $Ca_5Ti_3Fe_2O_{14}$[56] ($y = 0.20$, $n = 5$) has short-range order and is believed to have the same sequence as $Ca_4YFe_5O_{13}$.

2.4.5. Complex Cuprates.[58] $Ba_3La_3Cu_6O_{14+x}$[59] ($n = 1.5$) is tetragonal and has a $\sqrt{2}a_p \times \sqrt{2}a_p \times 3a_p$ cell size. The copper cations are found in CuO_4 square planes, CuO_5 square pyramids, and CuO_6 distorted octahedra. The compound is a well-ordered $m = 3$ phase. $BaLa_4Cu_5O_{14-\delta}$[60] ($n = 5$) is tetragonal and has a cell size that is roughly $\sqrt{5}a_p \times \sqrt{5}a_p \times 1a_p$. The copper cations are found in CuO_5 square pyramids and CuO_6 distorted octahedra. $La_{8-x}Sr_xCu_8O_{20-\delta}$[61] ($1.28 \le x \le 1.92$; $n = 2$) is orthorhombic and has a $\sqrt{2}a_p \times \sqrt{2}a_p \times 1a_p$ cell size. The copper cations form CuO_4 square planes, CuO_5 square pyramids, and CuO_6 elongated octahedra. $Sr_6La_2Cu_8O_{16}$[62] ($n = 1$) is tetragonal, has a $2\sqrt{2}a_p \times 2\sqrt{2}a_p \times 1a_p$ cell size, and contains copper cations in CuO_2 dumbbells, CuO_4 square planes, and CuO_5 square pyramids. $Sr_6La_2Cu_8O_{18-\delta}$[63,64] ($n = 1.33$) is tetragonal, has a $2\sqrt{2}a_p \times 2\sqrt{2}a_p \times 1a_p$ cell size, and has the same structure as $Sr_6La_2Cu_8O_{16}$ except that the copper cations exist exclusively in the CuO_4 square planes and CuO_5 square pyramids. The extra oxygen in the latter compound converts the coordination around copper from linear to square planar.

2.4.6. Calcium Manganates. $CaMnO_{3-x}$ phases that contain ordered microdomains[65,66] are known for overall oxygen contents of 2.80, 2.75,[67] 2.66, 2.56, and 2.50. More than one structure was observed in high-resolution electron microscopy at several of the oxygen contents. The manganese cations are found in MnO_5 square pyramids and MnO_6 octahedra, except for $CaMnO_{2.50}$ (section 2.4.1) in which the manganese cations are found exclusively in MnO_5 square pyramids.

3. AO_{3-x} Model of Oxygen-Deficient Perovskites

The polyhedral descriptions above do not convey adequately the structural similarity among the oxygen-deficient compounds. AO_{3-x} slices show the similarity and facilitate comparisons. The AO_{3-x} slices for $Ca_2Mn_2O_5$,[34,35] $LaSrCuGaO_5$,[16,17] $LaSrCuAlO_5$,[18,19] $La_2Ni_2O_5$,[36,37] YBa-

(56) Grenier, J.-C.; Pouchard, M.; Hagenmuller, P. *Struct. Bonding (Berlin)* **1981**, *47*, 1.

(57) Bando, Y.; Sekikawa, Y.; Nakamura, H.; Matsui, Y. *Acta Crystallogr., Sect A* **1981**, *37*, 723.

(58) The vacancy patterns are generally more complex than above owing to the diversity of copper coordination. The coordination of copper will be emphasized and the reader interested in the arrangement of defects is directed to the individual articles.

(59) Er-Rakho, L.; Michel, C.; Provost, J.; Raveau, B. *J. Solid State Chem.* **1981**, *37*, 151.

(60) Michel, C.; Er-Rakho, M.; Hervieu, M.; Pannetier, J.; Raveau, B. *J. Solid State Chem.* **1987**, *68*, 143.

(61) Er-Rakho, L.; Michel, C.; Raveau, B. *J. Solid State Chem.* **1988**, *73*, 514.

(62) Fu, W. T.; Ijdo, D. J. W.; Helmholdt, R. B. *Mater. Res. Bull.* **1992**, *27*, 287.

(63) Fu, W. T.; Xu, Q.; Verheijen, A. A.; van Ruitenbeek, J. M.; Zandbergen, J. W.; de Jongh, L. J. *Solid State Commun.* **1990**, *73*, 291.

(64) Fu, W. T.; Mijlhoff, F. C.; Ijdo, D. J. W.; Ponec, V. *Solid State Commun.*, in press.

(65) Reller, A.; Jefferson, D. A.; Thomas, J. M.; Beyerlein, R. A.; Poeppelmeier, K. R. *J. Chem. Soc., Chem. Commun.* **1982**, 1378.

(66) Reller, A.; Jefferson, D. A.; Thomas, J. M.; Uppal, M. K. *J. Phys. Chem.* **1983**, *87*, 913.

(67) Chiang, C. K.; Poeppelmeier, K. R. *Mater. Lett.* **1991**, *12*, 102.

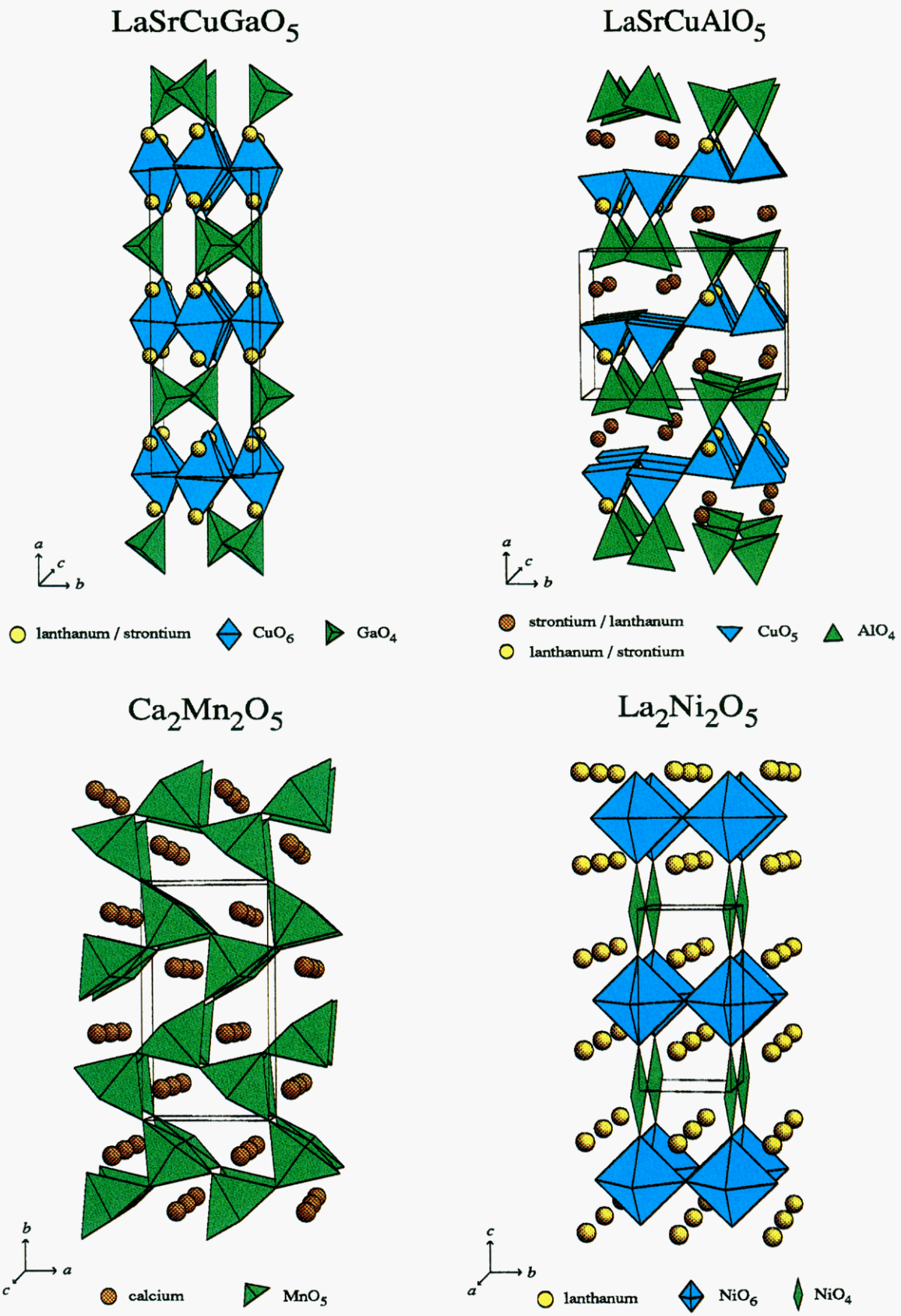

Plate I: **Figure 4** (upper left): structure of $LaSrCuGaO_5$. **Figure 5** (upper right): structure of $LaSrCuAlO_5$. **Figure 6** (lower left): structure of $Ca_2Mn_2O_5$. **Figure 7** (lower right): proposed (idealized) structure of $La_2Ni_2O_5$ after Vidyasagar et al.[37]

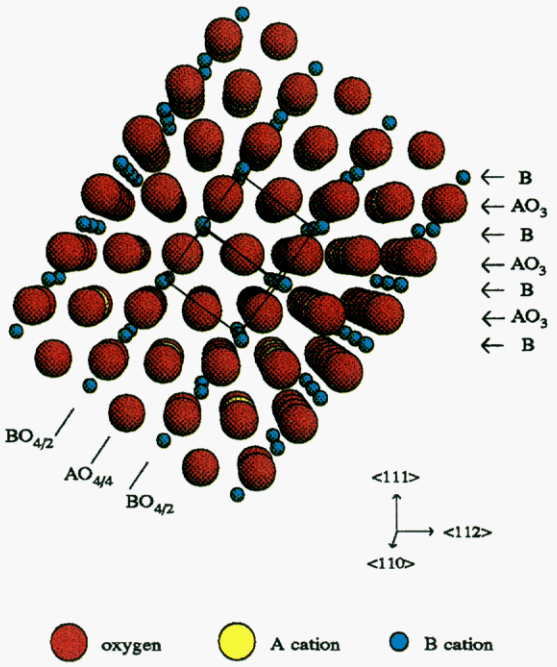

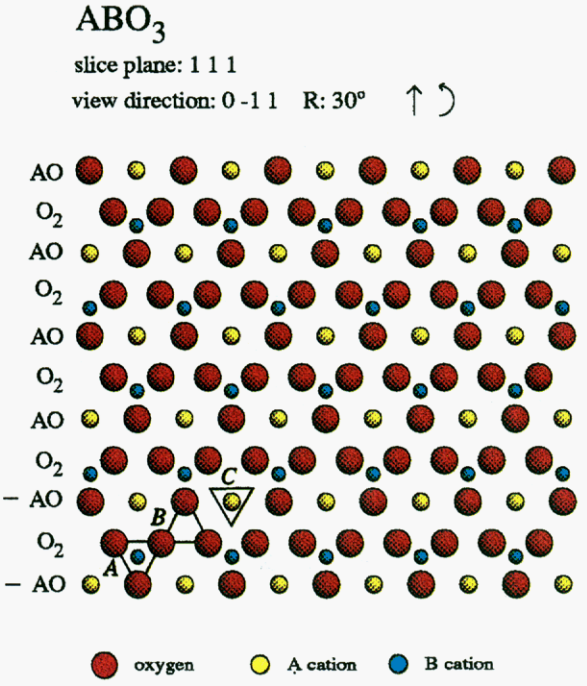

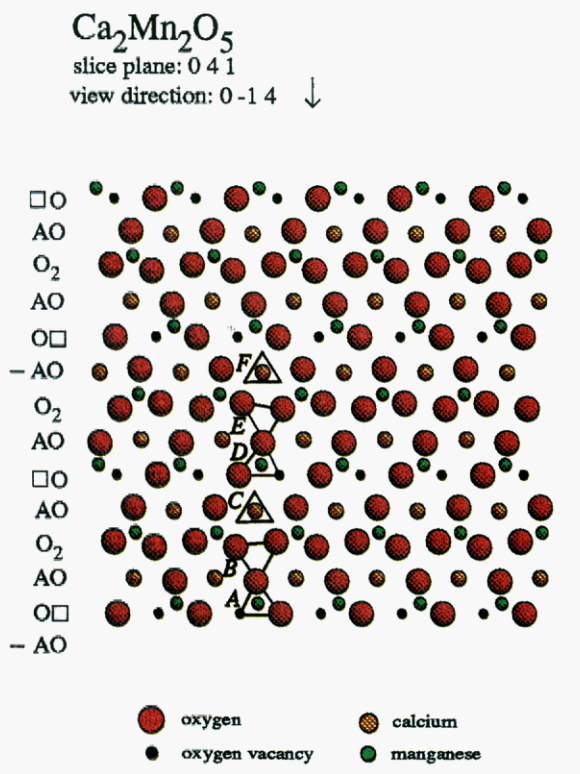

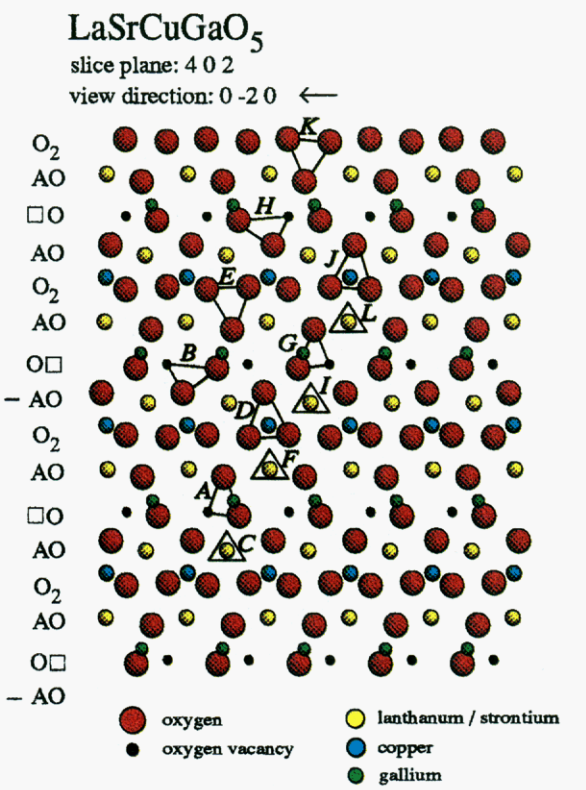

Plate II: **Figure 2** (upper left): perovskite structure shown as cubic-close-packed AO_3 layers. **Figure 16** (upper right): AO_3 slice of an ideal stoichiometric perovskite. **Figure 18** (lower left): AO_{3-x} slice of $Ca_2Mn_2O_5$. **Figure 19** (lower right): AO_{3-x} slice of $LaSrCuGaO_5$.

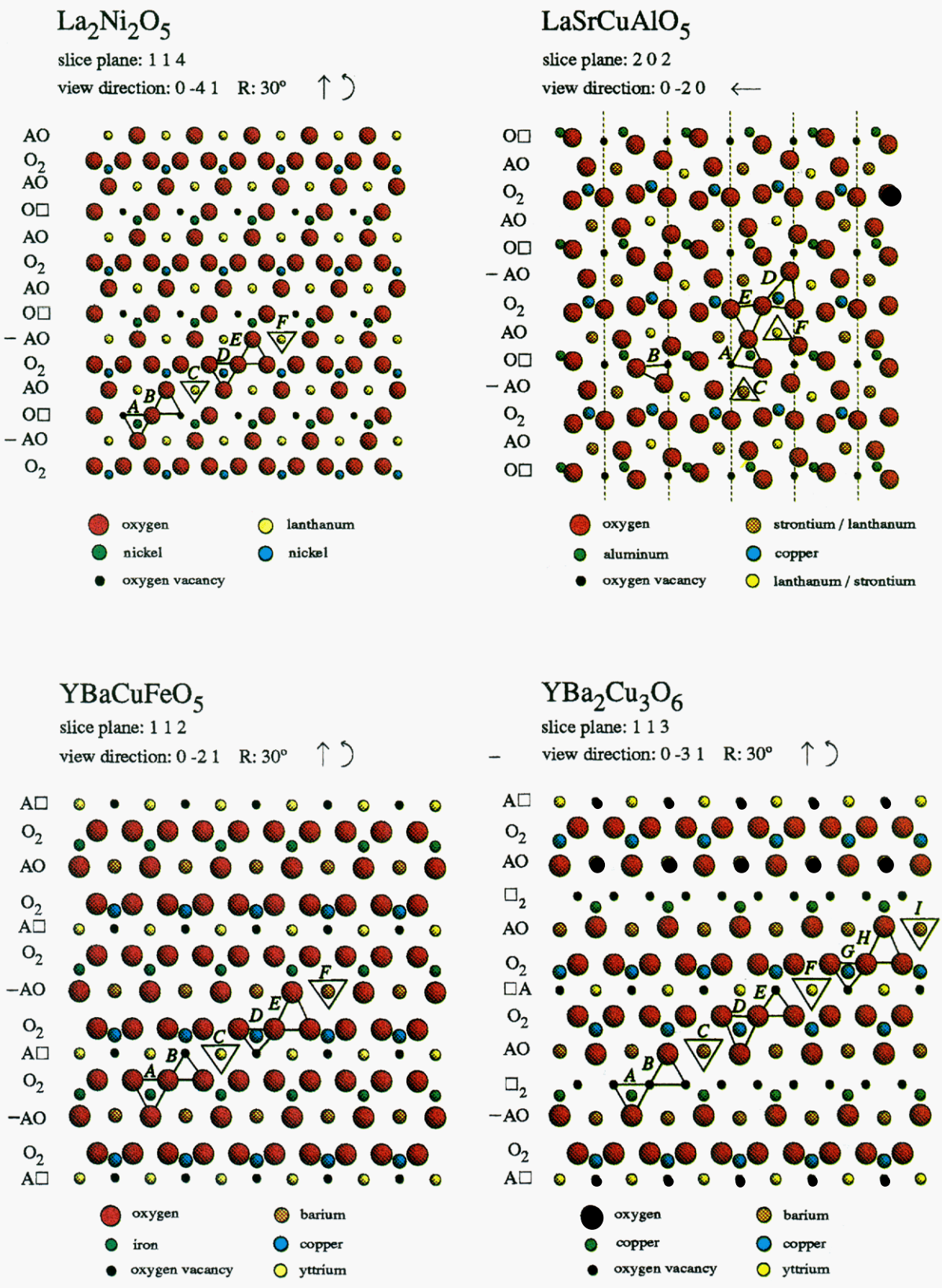

Plate III: **Figure 20** (upper left): AO_{3-x} slice of $La_2Ni_2O_5$. **Figure 21** (upper right): AO_{3-x} slice of $LaSrCuAlO_5$. The mirror operation, indicated by the dotted lines, is applied to layers *B*, *D*, and *F*. **Figure 22** (lower left): AO_{3-x} slice of $YBaCuFeO_5$. **Figure 23** (lower right): AO_{3-x} slice of $YBa_2Cu_3O_6$.

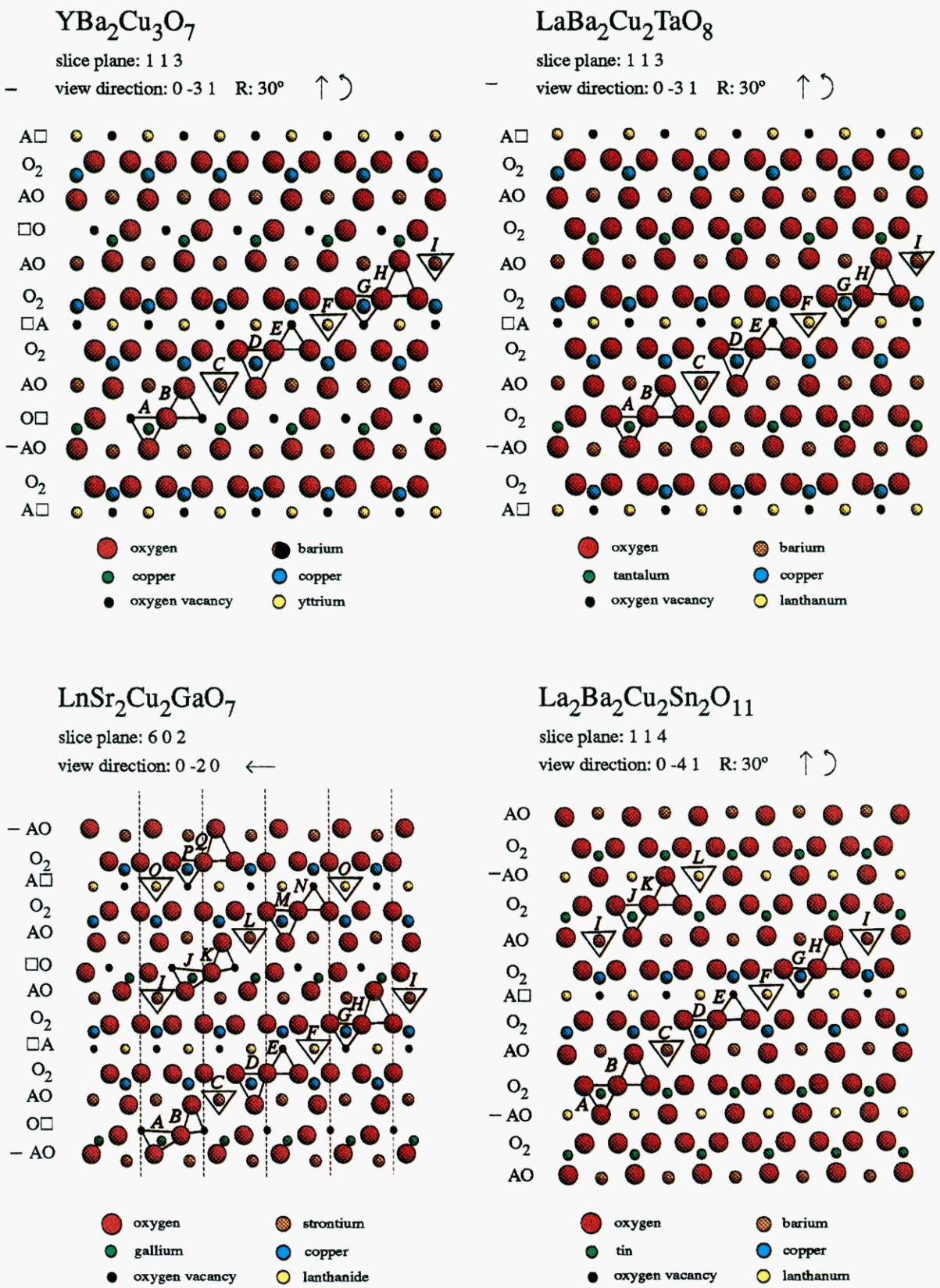

Plate IV: **Figure 24** (upper left): AO_{3-x} slice of $YBa_2Cu_3O_7$. **Figure 25** (upper right): AO_{3-x} slice of $LaBa_2Cu_2TaO_8$. **Figure 26** (lower left): AO_{3-x} slice of $LnSr_2Cu_2GaO_7$. The mirror operation, indicated by the dotted lines, is applied to layers *B*, *D*, *F*, *H*, *J*, *L*, *N*, and *P*. **Figure 27** (lower right): AO_{3-x} slice of $Ba_2La_2Cu_2Sn_2O_{11}$.

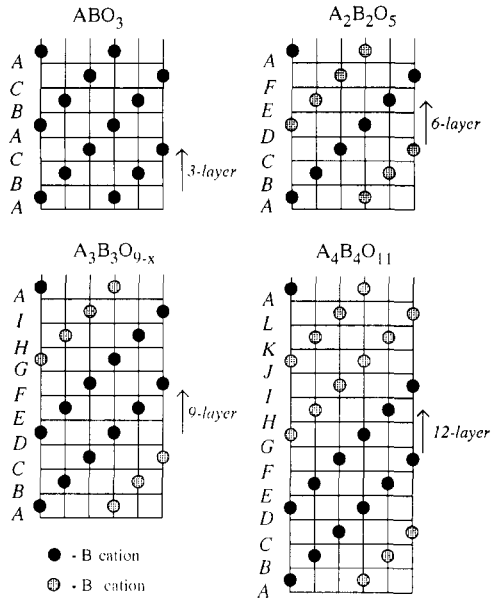

Figure 17. The B-cation arrangement perpendicular to the AO_3 layers. The $(110)_c$ plane is in the plane of the paper.

$CuFeO_5$,[20-24] $YBa_2Cu_3O_6$,[25-27] $YBa_2Cu_3O_7$,[4,5] $LnSr_2Cu_2GaO_7$,[31,32] $LaBa_2Cu_2TaO_8$,[28-30] and $Ba_2La_2Cu_2Sn_2O_{11}$[33] are displayed, described, and discussed, in addition the slices for $Ca_2Co_2O_5$,[38] $LaSr_2Fe_3O_8$,[39-42] and $Ca_4Ti_2Fe_2O_{11}$[43] are described and discussed. For each compound, the slice plane shown corresponds to the (111) plane in cubic perovskite. All slices have been rotated so that the sequence of rows is ...AO O_2 AO O_2 AO... from bottom to top of the figure (see Figure 16), for example. The view direction is indicated by an arrow. In some of the figures, the direction of the arrow must be rotated by the amount shown. After the arrow has been rotated it is parallel to the view direction. The B cations are also shown and lie above triangles formed by three oxygen atoms (or a combination of oxygen atoms and oxygen vacancies) from the AO_{3-x} slice below.

3.1. Description of AO_{3-x} Slices and Construction of Structures. A 111 slice of the perovskite structure is shown in Figure 16. Each A cation is surrounded by six oxygen atoms in a hexagonal net. The B cations reside above each slice in trigonal antiprisms (octahedral holes) formed by three oxygen atoms from the layer (slice) below and three from the layer above (not shown). The arrangement of oxygen atoms around the B cations is designated 3 + 3, where the first number refers to the oxygen atoms from the layer below and the second to the oxygen atoms from the layer above. Figure 16 shows one AO_3 layer and indicates how identical layers are stacked; to form the three-dimensional solid, three layers identical to that shown in Figure 16 are stacked such that triangle B is directly above triangle A as viewed down ⟨111⟩ (perpendicular to the page) and forms a trigonal antiprism, and triangle C is above triangle B and forms a trigonal antiprism. Successive layers are stacked in the sequence *ABC ABC* to form a cubic-close-packed lattice. Note that *A*, *B*, *C*, and so on refer to layer types, and A and B refer to cations. The AO_3 B AO_3 B AO_3 stacking sequence (perpendicular to the view just described) is illustrated in Figure 2. An elevation of the perovskite structure is shown in the upper left corner of Figure 17. The view direction is identical to that in Figure 2. The close-packed layers are labeled *A*, *B*, and *C*, and the B-cation pattern on the (110) face of cubic perovskite structure is shown. This view was originally introduced by Ward and Katz[68] and its use was promoted by Wells.[69]

As is the case for stoichiometric perovskites, all oxygen-deficient compounds can be viewed as derived from AO_{3-x} layers that are stacked in an *ABC ABC* sequence to give a cubic-close-packed structure. In contrast to stoichiometric perovskites, the B cations reside in six-, five-, four-, or two-coordinate interstices formed from a combination of oxygen atoms and vacancies from the layers above and below (6 = 3 + 3, 5 = 3 + 2□, 4 = 2□ + 2□, and 2 = 1□□ + 1□□). For four-coordinate metal atoms (2□ + 2□), the vacancies can be cis or trans in the octahedron (trigonal antiprism) around the atom. If the vacancies are cis, which results from removal of oxygen atoms from $[110]_c$ rows, the metal atom has a tetrahedral coordination environment. If the vacancies are trans, which results from removal of oxygen atoms from $[100]_c$ rows, the metal atom has a square planar coordination environment.

3.2. B-Cation Patterns. Figure 17 shows the B-cation patterns for $A_2B_2O_5$ ($m = 2$), $A_3B_3O_{9-x}$ ($m = 3$), and $A_4B_4O_{11}$ ($m = 4$) oxygen-deficient perovskites. In $A_2B_2O_5$ compounds, there is a six-layer repeat perpendicular to the AO_{3-x} layers if B′ and B″ are not the same ($LaSrCuGaO_5$,[16,17] $LaSrCuAlO_5$,[18,19] and $YBaCuFeO_5$[20-24]), and a three-layer repeat if B′ and B″ are the same ($Ca_2Mn_2O_5$,[34,35] $La_2Ni_2O_5$,[36,37] and $Ca_2Co_2O_5$[38]). Note that the repeat refers only to the B-cation pattern and may be longer owing to arrangement of vacancies (as discussed below). In the $A_3B_3O_{9-x}$ compounds, there is a nine-layer repeat perpendicular to the AO_{3-x} layers. In the $A_4B_4O_{11}$ compound $Ba_2La_2Cu_2Sn_2O_{11}$,[52] there is a 12-layer repeat perpendicular to the AO_{3-x} layers. The views in Figure 17 not only demonstrate the B-cation pattern, they help emphasize the manner in which AO_{3-x} layers stack; the rows of B cations parallel to $\langle 110 \rangle_c$ are staggered from one layer to the next.

3.3. Choice of AO_{3-x} Slices. It is not in general true that one unique $(111)_c$ slice exists for every oxygen-deficient compound. For example, in the case of $LaSr_2Cu_2GaO_7$, both the 602 and 620 planes correspond to {111} planes in cubic perovskite; however, there are two distinct 620 planes that must be stacked alternately to generate the structure, whereas there is one unique 602 plane, which can be stacked (after a mirror operation) to generate the three-dimensional structure. For this review, one unique slice plane has been chosen for each compound such that it can be stacked to generate the three-dimensional compound.

3.4. AO_{3-x} Description of $A_mB_mO_{3m-x}$ Perovskite Structures. Some of the compounds have long stacking sequences owing to A-cation, B-cation, and oxygen vacancy order. If small topological transformations[70] and oxygen vacancies are ignored, the compounds are cubic-closest-packed and would have an *ABC* sequence if A′ and A″ were the same and B′ and B″ were the same. As stated by Andersson and Hyde,[70] "a topological transformation involves a (continuous) nonrigid motion that changes one figure into another so that each point in the first has a corresponding point in the second. No points (atoms) are

(68) Katz, L.; Ward, R. *Inorg. Chem.* **1964**, *3*, 205–211.
(69) Wells, A. F. *Structural Inorganic Chemistry*, 5th ed.; Oxford: New York, 1984.
(70) Hyde, B. G.; Andersson, S. In *Inorganic Crystal Structures*; Wiley: New York, 1989; Chapter 9.

lost or generated in the transformation, although distances and orientation change (not by very much in the cases of interest to us)." The parentheses are theirs and not ours. For our use, we will imagine that each atom of a slice is connected to all of its nearest neighbors. If two slices are topologically related, as is the case in several instances, no connections need be broken to transform the arrangement (positions) of the ions and vacancies in one slice to that in the other.

3.4.1. m = 2. Of the six structure types analyzed, four have one-half of their oxygen atoms removed from every other O_2 row in the AO_{3-x} slice, denoted O□ or □O depending on the orientation of the oxygen atom and oxygen vacancy, one has one-half removed from every other AO row, denoted A□ or □A depending on the orientation of the A cation and oxygen vacancy, and one is more complex. Of the first four, two have vacancies that form lines perpendicular to the AO rows, and two have vacancies that zig-zag perpendicular to the AO rows. The presentation will thus be broken into four sections.

$Ca_2Mn_2O_5$[34,35] (Figure 18) and $LaSrCuGaO_5$[16,17] (Figure 19): In stark contrast to the polyhedral representations of $Ca_2Mn_2O_5$ and $LaSrCuGaO_5$, which are distinctly different (see Figures 4 and 6), their AO_{3-x} slices are topologically related.[70] In each slice, one-half of the oxygen atoms are removed from every other O_2 row and the rows of vacancies zig-zag from the bottom to the top of the figure (perpendicular to the AO rows). Note that in Table I the interchange of the oxygen atom and oxygen vacancy position from row to row is shown as O□ and □O. The slices have exactly the same sequence of ions and vacancies in each row and are constructed from exactly the same sequence of rows (shown at the left hand side of each figure). The essential difference in the two structures is the manner in which successive AO_{3-x} layers (slices) are stacked. In the manganese compound, the layers stack such that each d^4 Mn^{3+} has five oxygen atoms and one vacancy around it (2□ + 3 and 3 + 2□). This produces a six-layer sequence. In the copper gallate, the layers stack such that each copper has six oxygen atoms around it (3 + 3), and each gallium has four oxygen atoms and two vacancies around it (2□ + 2□). Although the arrangement of the B cations produces a six-layer sequence, the position of the vacancies from layer to layer produces a 12-layer repeat overall. The vacancies are cis in the octahedron that results from the O_2□ Ga O_2□ stacking parallel to $\langle 111 \rangle_c$. Note that the gallium atoms are displaced away from the vacancies and are in pseudotetrahedral coordination.

$La_2Ni_2O_5$[36,37] (Figure 20) and $LaSrCuAlO_5$[18,19] (Figure 21): As in the compounds above, the slices are topologically related. In each slice, one-half of the oxygen atoms are removed from every other O_2 row and the rows of vacancies form a line perpendicular to the AO rows. In both compounds one-half of the B cations are (pseudo)-six-coordinate (3 + 3)[71] and one-half are four-coordinate (2□ + 2□), but, in the aluminum compound, the aluminum is in (roughly) tetrahedral coordination, and, in the nickel compound, the nickel is in square planar coordination. The essential difference between the structures is the manner in which the layers are stacked. In the nickel compound, the vacancies are trans in the octahedron that results from the O_2□ Ni O_2□ stacking parallel to $\langle 111 \rangle_c$, and in the aluminum compound, the vacancies are cis in the octahedron that results from the O_2□ Al O_2□ stacking parallel to $\langle 111 \rangle_c$. Note that the aluminum atoms are displaced away from the vacancies. Each compound has a six-layer repeat. Successive layers in the aluminum compound are generated by a mirror operation. The mirror plane is perpendicular to the line of vacancies. Before triangle *B* is stacked above triangle *A* a mirror operation must be performed on it. The operation prior to stacking *B* on top of *A* results in the cis orientation of the vacancies, rather than the trans arrangement that would occur if *B* were stacked on A without the mirror operation. The operation is applied to layers *B*, *D*, and *F*.

$YBaCuFeO_5$[20-24] (Figure 22): In contrast to the $A_2B_2O_5$ compounds above, all of the oxygen atoms are removed from every other AO row rather than half from every O_2 row. Similar to $LaSrCuAlO_5$ and $La_2Ni_2O_5$, the rows of vacancies form a line perpendicular to the AO rows. Each copper and iron are five coordinate (2□ + 3 and 3 + 2□). There is a six-layer stacking sequence. The stacking of successive layers follows the same pattern as in $La_2Ni_2O_5$.

$Ca_2Co_2O_5$[38] (not shown): The vacancy pattern in each slice is complex and has a repeat of AO O□ AO $O_{1.5}$□$_{0.5}$ A□ $O_{1.5}$□$_{0.5}$ AO O_2 AO O_2 $AO_{0.5}$□$_{0.5}$ O_2 AO. The slices stack such that each d^6 cobalt has five oxygen atoms around it (2□ + 3 and 3 + 2□). Because the structure was inferred from electron diffraction data and lattice constants determined by powder X-ray diffraction, it is in question. The slice will not be shown here. There is a possibility that the cobalt is six and four coordinate rather than all five-coordinate.

3.4.2. m = 3. $YBa_2Cu_3O_6$[25-27] (Figure 23), $YBa_2Cu_3O_7$[4,5] (Figure 24), and $LaBa_2Cu_2TaO_8$[28-30] (Figure 25): In the slices of all three compounds, all of the oxygen atoms are removed from every third AO row and the vacancies zig-zag perpendicular to the AO rows. Each compound has a nine-layer stacking sequence. The layers stack in the same manner as for $La_2Ni_2O_5$ and $YBaCuFeO_5$, although the sequence is longer (nine versus six layers). In $YBa_2Cu_3O_6$, all of the oxygen atoms are also removed from every third O_2 row, and the layers stack such that the copper atoms in the $CuO_{4/2}$ planes (see Figure 10) are five-coordinate (3 + 2□ and 2□ + 3), and the dumbbell copper atoms are two-coordinate (1□□ + 1□□) in the interleaved Cu□$_{4/2}$ plane. In $YBa_2Cu_3O_7$, one-half of the oxygen atoms are removed from every third O_2 row and the vacancies zig-zag perpendicular to the AO rows. The layers stack such that the in-plane copper atoms are five-coordinate (3 + 2□ and 2□ + 3) and the chain copper atoms are four-coordinate (2□ + 2□). The vacancies are trans in the O_2□ Cu O_2□ sequence. In $Ba_2LaCu_2TaO_8$, the oxygen atoms are removed only from every third AO row, and the slices stack such that the copper atoms are five-coordinate (3 + 2□ and 2□ + 3) and the tantalum atoms are six-coordinate (3 + 3).

$LnSr_2Cu_2GaO_7$[31,32] (Figure 26) and $YBa_2Cu_3O_7$ (Figure 24): $LnSr_2Cu_2GaO_7$ is topologically related to $YBa_2Cu_3O_7$. In both compounds all of the oxygen atoms are removed from every third AO row, one-half of the oxygen atoms are removed from every third O_2 row, the vacancies from the AO rows zig-zag from row to row as do those from the O_2 rows, and the slices stack such that the copper atoms are five-coordinate (3 + 2□ and 2□ + 3) and the gallium or copper atoms are four-coordinate (2□ + 2□). The difference between the structures is the manner in which the

(71) One of the apical copper–oxygen distances in the aluminate is 2.954 (8) Å. The coordination around copper is actually square pyramidal.

layers are stacked. In $LnSr_2Cu_2GaO_7$, similar to $LaSrCuAlO_5$ (see Figure 21), a mirror operation is performed on every other slice before it is stacked, that is, on layers *B*, *D*, *F*, *H*, *J*, *L*, *N*, and *P*. The effect of the mirror operation is to make the vacancies cis in the $O_2\square$ Ga $O_2\square$ sequence. If the mirror operation were not performed, the vacancies would be trans as they are in the $O_2\square$ Cu $O_2\square$ sequence in $YBa_2Cu_3O_7$. Owing to order of B cations and oxygen vacancies, the stacking sequence for $LnSr_2Cu_2GaO_7$ has an 18-layer repeat; see Figure 26.

$LaSr_2Fe_3O_8$[39-42] *(not shown)*: The oxygen atoms and iron forms are disordered in such a way that there is not one unique slice that can be stacked to generate the structure. In contrast to the other $A_3B_3O_{9-x}$ compounds, all of the oxygen atoms are removed from every third O_2 row rather than from every third AO row. The layers stack such that two out of three iron atoms are six-coordinate (3 + 3) and the one out of three is four-coordinate (2□ + 2□). The vacancies form a line perpendicular to the AO rows and are cis in each $O_2\square$ Fe $O_2\square$ sequence. There is an 9-layer stacking sequence.

4.4.3. m = 4. $Ba_2La_2Cu_2Sn_2O_{11}$[33] *(Figure 27)*: All of the oxygen atoms from every fourth AO row are removed, and the vacancies in the A□ rows form a line perpendicular to the AO rows, which is similar to $LaBa_2Cu_2TaO_8$ where the oxygen atoms in every third AO row are removed. The copper atoms are five-coordinate (3 + 2□ and 2□ + 3) and the tin atoms are six-coordinate (3 + 3). The stacking sequence follows the same pattern as $La_2Ni_2O_5$, $YBaCuFeO_5$, $YBa_2Cu_3O_6$, $YBa_2Cu_3O_7$, and $LaBa_2Cu_2TaO_8$ but has a longer repeat (12 versus 6 and 9 layers).

$Ca_4Ti_2Fe_2O_{11}$[43] *(not shown)*: The structural features have been investigated only with X-ray diffraction (to determine lattice constants) and electron diffraction.[51] Owing to the lack of a complete structure determination, a slice is not presented here. On the basis of the vacancy pattern proposed from electron diffraction (section 2.4.3), all of the oxygen atoms are removed from every fourth O_2 row, which is similar to $LaSr_2Fe_3O_3$ where oxygen atoms are removed from every third O_2 row. The slices stack such that the titanium and one-half of the iron atoms are six-coordinate (3 + 3) and the other half of iron atoms are four-coordinate (2□ + 2□). The vacancies form a line perpendicular to the AO rows are cis in each $O_2\square$ Fe $O_2\square$ sequence. There is a 12-layer stacking sequence.

4. Discussion

4.1. Structural Similarity among Oxygen-Deficient Perovskites: ABO_{3-x} Slices. In oxygen-deficient perovskites with the same general formula and structure type, the similarity of the arrangement of ions is not always obvious; however, compounds that are dissimilar in coordination polyhedra, A-cation coordination numbers, and B-cation coordination numbers do indeed have structural similarity because, as presented above, they are formed from topologically or otherwise related (see below) AO_{3-x} layers; see Table I. Metal oxides are quite ionic; therefore, their stability is dictated primarily by electrostatic interactions between ions.[72] The analogous arrangement of ions in the AO_{3-x} slices indicates that these ionic compounds are not only structurally similar but are also energetically similar. The energetics of these compounds have not been explored based on an AO_{3-x} model, but this would be useful and informative.

The pairs of compounds 1-3, 1-4, 2-3, and 2-4, where $Ca_2Mn_2O_5$ is 1, $LaSrCuGaO_5$ is 2, $La_2Ni_2O_5$ is 3, $LaSrCuAlO_5$ is 4, have slices that are closely but not topologically related. In all of the compounds one oxygen atom fully occupies one of two sites in an O□ row and the other site is vacant; see Table I. The rows that make up the slices are identical in pairs 1-3, 1-4, 2-3, and 2-4 except that from one compound to the next the positions of the oxygen atoms and the vacancies within an O□ row have been interchanged. For example, in $LaSrCuAlO_5$ (4) the sequence in the O□ rows is O□O□O□ whereas in $LaSrCuGaO_5$ (2) the sequence is O□O□O□ in half of the O□ rows, but is □O□O□O in the other half (denoted □O), that is, the position of the oxygen atoms and vacancies have been interchanged in half of the O□ rows in gallate (2) relative to the aluminate (4). The relationships among the other pairs are analogous and are explored in detail in the next section.

4.1.1. m = 2. $Ca_2Mn_2O_5$,[34,35] $LaSrCuGaO_5$,[16,17] $La_2Ni_2O_5$,[36,37] and $LaSrCuAlO_5$[18,19] appear dissimilar in overall structure, B-cation coordination numbers (5, 5; 6, 4; 6, 4; 5, 4), and A-cation coordination numbers (10, 10; 8, 8; 10, 10; 8, 9), but their AO_{3-x} slices all have an AO O□ AO O_2 AO [O□] AO O_2 pattern; see Table I. In this notation, [O□] denotes that the arrangement is either O□ ($La_2Ni_2O_5$, $LaSrCuAlO_5$) or □O ($Ca_2Mn_2O_5$, $LaSrCuGaO_5$). The slices for the $Ca_2Mn_2O_5$ and $LaSrCuGaO_5$ are topologically related, as are the slices for $La_2Ni_2O_5$ and $LaSrCuAlO_5$. This relationship means they are made up an identical sequence of rows; see Table I. As described above, the manganate and the gallate are related to the nickelate and the gallate by an interchange of oxygen atom and oxygen vacancy positions in O□ rows. The similarity of the AO_{3-x} slices emphasizes the structural similarity of the compounds, as shown in sections 4.4.1. $YBaCuFeO_5$[20-24] (5, 5; 8, 12) differs from the others previously described in that the oxygen atoms are removed from an AO row, A□ O_2 AO O_2, rather than an O_2 row.

4.1.2. m = 3, 4. The *m* = 3 compounds show remarkable similarity also; see Table I. $YBa_2Cu_3O_7$[4,5] (5, 5, 4; 8, 10, 10) and $LnSr_2Cu_2GaO_7$[31,32] (5, 5, 4; 8, 8, 8) have oxygen atoms removed in a different manner, along $[100]_c$ versus along $[110]_c$, yet both have an AO O□ AO O_2 □A O_2 AO □O AO O_2 A□ O_2 sequence and their AO_{3-x} slices are topologically related. The sequence for $YBa_2Cu_3O_6$[25-27] (5, 5, 2; 8, 8, 8) differs from that for $YBa_2Cu_3O_7$ and $LnSr_2Cu_2GaO_7$ only in replacement of O□ with $\square_2$, that is, AO ($\square_2$) AO O_2 □A O_2 AO ($\square_2$) AO O_2 A□ O_2, where parentheses indicate a replacement of one row with another rather than the interchange of ionic position, which is indicated by square brackets. $LaBa_2Cu_2TaO_8$[28-30] (5, 5, 6; 8, 12, 12) replaces O□ in $YBa_2Cu_3O_7$ and $LnSr_2Cu_2GaO_7$ with O_2 to form its AO_{3-x} pattern, AO (O_2) AO O_2 □A O_2 AO (O_2) AO O_2 A□ O_2. The defect pattern in $LaSr_2Fe_3O_8$[39-42] (6, 6, 4; 12, 10, 10) is also comparable to the above; the A□ in the sequence for $YBa_2Cu_3O_7$ and $LnSr_2Cu_2GaO_7$ has been replaced by AO to yield an AO O□ AO O_2 (AO) O_2 sequence. The *m* = 4 compound $Ba_2La_2Cu_2Sn_2O_{11}$[33] (5, 5, 6, 6; 12,

(72) See, for example: Rao, C. N. R.; Gopalkrishnan, J. In *New Directions in Solid State Chemistry*; Cambridge University Press: New York, 1989; pp 4-10.

(73) Dowty, E. *ATOMS: A Computer Program for Displaying Atomic Structures, IBM-PC Version 2.1*; Kingsport, TN, 1991. For more information, write to Eric Dowty, 512 Hidden Valley Road, Kingsport, TN 37663.

12, 12, 8) is related to $LaBa_2Cu_2TaO_8$. The sequence differs by the insertion of AO O_2, which reflects the presence of an additional ABO_3 unit. The sequence is AO O_2 (AO O_2) AO O_2 A□ O_2.

4.2. B-Cation Influence on AO_{3-x} Stacking Sequence. Although the cohesive energy of a metal oxide is dominated by spatially isotropic electrostatic interactions,[72] the arrangement of the vacancies within a slice and from slice to slice is largely controlled by spatially anisotropic (directional) covalent interactions of the B and O ions. The sizes, electronic configurations, and coordination preferences of the B cations control the arrangement of vacancies around each B cation and, along with A-cation size and coordination preferences coordination preferences, control the manner in which AO_{3-x} layers stack. The physical and chemical differences in A and B cations from compound to compound account for the variety of known vacancy patterns.

4.2.1. m = 2. $Ca_2Mn_2O_5$[34,35] and $LaSrCuGaO_5$:[16,17] The structural differences between $Ca_2Mn_2O_5$ and $LaSrCuGaO_5$ demonstrate the influence that electronic configurations and coordination preferences of the B cations (5, 5 versus 6, 4) have on the manner in which topologically related slices stack. In $Ca_2Mn_2O_5$, the manganese cations are all d^4 Mn^{3+} and prefer five-coordinate square pyramidal sites (3 + 2□ and 2□ + 3) rather than six-coordinate and four-coordinate sites (3 + 3 and 2□ + 2□) as in $LaSrCuGaO_5$. The slices stack such that the manganese cations are five-coordinate. In $LaSrCuGaO_5$, the copper cations are d^9 Cu^{2+}, which can adopt six-, five- or four-coordination, and gallium cations are d^{10} Ga^{3+}, which prefer small, spherical pseudotetrahedral sites. There are many examples of copper(II) in square-pyramidal or square-planar coordination, but in this case the coordination preference of the smaller gallium ions cause the defects to cluster around them (2□ + 2□), and the copper ions remain six-coordinate (3 + 3). The slices stack such that the copper cations are six-coordinate and gallium cations are four-coordinate.

$La_2Ni_2O_5$[36,37] and $LaSrCuAlO_5$:[18,19] The structural differences between $La_2Ni_2O_5$ and $LaSrCuAlO_5$ illustrate the effect that electronic configurations of the B cations have on that manner in which the slices stack. The AO_{3-x} slices are topologically related (section 3.4.1), yet the environments around the B cations are different. In $La_2Ni_2O_5$, the nickel cations are d^8 Ni^{2+}. The cations adopt elongated octahedral (3 + 3) and square planar coordination (2□ + 2□). In $LaSrCuAlO_5$, the copper cations are d^9 Cu^{2+} and the aluminum cations are d^{10} Al^{3+}. Similar to the gallium cations in $LaSrCuGaO_5$, the small spherical (closed-valence shell) aluminum cations cause the defects to cluster around them. The aluminum cations adopt (pseudo)tetrahedral coordination (2□ + 2□) and the copper cations adopt elongated octahedral coordination (3 + 3). $LaSrCuAlO_5$ and $La_2Ni_2O_5$ differ in that the vacancies are trans in the $NiO_4□_2$ octahedron, which give rise to a square planar environment, and are cis in the $AlO_4□_2$ octahedron, which give rise to a tetrahedral environment. The difference in coordination geometry and stacking sequence is caused by the difference in electronic configuration of the Ni^{2+} and the Al^{3+} ion, d^8 versus d^{10}.

$LaSrCuGaO_5$,[16,17] $La_2Ni_2O_5$,[36,37] and $LaSrCuAlO_5$:[18,19] The differences in stacking sequences for these three $A_2B_2O_5$ compounds, which have (pseudo)-six-coordinate (3 + 3) and four-coordinate ions (2□ + 2□), also exemplify the effect that different electronic configurations of the B cations have on the stacking sequence. $La_2Ni_2O_5$ contains d^8 Ni^{2+}, $LaSrCuGaO_5$ contains d^9 Cu^{2+} and d^{10} Ga^{3+}, and $LaSrCuAlO_5$ contains d^9 Cu^{2+} and d^{10} Al^{3+}. The difference in coordination preference of d^8 versus d^{10} ions explains the difference between the first and the last two, as discussed previously. The difference between the gallate and aluminate is one of the size of the M^{3+} ions. The aluminum ions are smaller therfore more charge dense than the gallium ions, and each attracts one of the apical oxygen atoms around each copper ion and deprives the copper ion of its sixth near-neighbor oxygen atom. The larger size of the gallium ions allows the sixth oxygen atom to complete the elongated octahedron around each copper cation. The size difference is probably responsible for the different stacking sequence as well.

4.2.2. m = 3 and 4. The differences in the stacking sequences of $A_3B_3O_{9-x}$ and $A_4B_4O_{11}$ further attest to the dominant role the B-cation electronic configuration has in the determination of the sequence. The m = 3 and 4 cuprates are either more oxygen deficient (n is less) or contain larger B″ ions compared to the m = 2 compounds. The result is that copper is five-coordinate in these examples. All contain copper–oxygen double layers in which CuO_5 square pyramids share vacancies and form CuO_5–□–CuO_5 units (3 + 2□ and 2□ + 3 stacking) perpendicular to the copper–oxygen layers. The presence of such units as well as the electronic configuration of the B″ ion control the stacking sequences. $YBa_2Cu_3O_7$[4,5] and $LaSr_2Cu_2GaO_7$[31,32] have similar AO_{3-x} slices, see section 4.4.2, and both have five-coordinate copper, but d^8 Cu^{3+} is square planar (2□ + 2□) whereas d^{10} Ga^{3+} is pseudotetrahedral (2□ + 2□). As discussed above, the electronic differences of the B″ cations cause the defects to be trans in the Cu^{3+} case and cis in the Ga^{3+} case, which gives rise to different stacking sequences. The stacking sequences for $YBa_2Cu_3O_6$[25–27] and $YBa_2Cu_2TaO_8$[28–30] are the same as for $YBa_2Cu_3O_7$[4,5] (section 3.4.2) and indicate the influence of the five-coordinate d^9 Cu^{2+} as well as two-coordinate d^{10} Cu^{1+} (1□□ + 1□□) and six-coordinate d^0 Ta^{5+} (3 + 3).

The stacking sequence in $LaSr_2Fe_3O_8$[39–42] reflects the preference of iron for two six-coordinate and one four-coordinate (3 + 3, 3 + 3, and 2□ + 2□) d^5 Fe^{3+} ion per formula unit rather than two five-coordinate and one six-coordinate ion (3 + 2□, 2□ + 3, and 3 + 3) as in the $LaBa_2Cu_2TaO_8$. The stacking sequence in $Ba_2La_2Cu_2Sn_2O_{11}$[33] indicates the strong octahedral coordination preference (3 + 3) of the large d^{10} Sn^{4+} ion and the preference for two copper atoms to share a vacancy (3 + 2□ and 2□ + 3) rather than have six- and four-coordinate copper ions (3 + 3 and 2□ + 2□).

4.3. A-Cation Influence on AO_{3-x} Stacking Sequence. This size and coordination preferences of the A cations can also influence the stacking sequence. In compounds that contain vacancies in some but not all $AO_{4/4}$ layers, the A-cation sites have different coordination numbers and environments. For example, $Ca_2Mn_2O_5$[34,35] and $YBaCuFeO_5$[20–24] have B cations that are exclusively five-coordinate, but there is a large size difference between yttrium (1.16 Å) and barium (1.51 Å) and no size difference between the calcium atoms (1.34 Å). The different stacking sequence between the first two can be attributed to the coordination environment needs of the A sites (10, 10 versus 8, 12). The AO_{3-x} layers in $YBaCuFeO_5$ are stacked such that the A-cation sites are

12- and 8-coordinate. The sites are occupied by barium and yttrium respectively. The AO_{3-x} layers in $Ca_2Mn_2O_5$ are stacked such that the A-cation sites are 10-coordinate, and the sites are occupied by calcium. $YBa_2Cu_3O_7$,[4,5] $LaBa_2Cu_2TaO_8$,[28-30] and $La_2Ba_2Cu_2Sn_2O_{11}$[33] also contain $AO_{4/4}$ vacancies, A-cation coordination differences (8, 10, 10; 8, 12, 12; 8, 12, 12, 12), and ordered A-cations. The layers stack such that the different coordination preferences of the A cations are met.

5. Conclusions

When viewed as cubic-closed-packed AO_{3-x} layers, the structural and energetic similarities of oxygen-deficient perovskites are evident. Compounds that contain cations with different A- and B-cation coordination numbers are formed from AO_{3-x} layers that are topologically related or that are related by interchange of an oxygen atom and an oxygen vacancy. The sizes and electronic configurations of the B cations in addition to the sizes and coordination preferences of the A cations influence the manner in which AO_{3-x} layers are stacked. More complex structures are amenable to AO_{3-x} analysis but may not have one unique slice that can be stacked to generate the structure. In this case, the slices needed to generate the structure have to be identified and stacked properly. Through analysis of AO_{3-x} slices, one should be able to predict and understand structures that contain new vacancy patterns. Three-dimensional structures, especially those that contain two-dimensional features such as the high-temperature cuprate superconductors, should be analyzed along several crystallographic directions. Akin to the similarities seen in the *structures* of oxygen-deficient perovskites, similarities in *bonding*, *physical properties*, and other phenomena important in condensed matter physics may be evident when two-dimensional solid-state materials are viewed in directions other than parallel and perpendicular to the direction of greatest anisotropy.

Acknowledgment. This work was funded by the National Science Foundation and the Science and Technology Center for Superconductivity (NSF-DMR-9120000). The polyhedral representations and the AO_{3-x} slices were drawn with ATOMS,[73] an inexpensive commercial software package.